Engineering Failure Analysis 156 (2024) 107834

Contents lists available at ScienceDirect

Engineering Failure Analysis

journal homepage: www.elsevier.com/locate/engfailanal

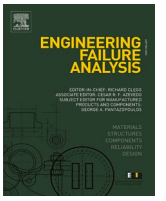

Holistic estimation and sensitivity-based experiment design method of composite laminate first-ply failure models using statistical approaches

László Kovács [a,b,*], Márton Bugár-Mészáros [a], Gábor Romhány [b]

[a] eCon Engineering Kft., Kondorosi str. 3, H-1116 Budapest, Hungary
[b] University of Technology and Economics, Department of Polymer Engineering, Budapest, Hungary

ARTICLE INFO

Keywords:
Composites
Maximum likelihood
Sensitivity
Identifiability
Failure

ABSTRACT

In this paper, a probabilistic approach is presented to simultaneously evaluate all strength and additional fitting parameters of a pre-selected composite first-ply failure model using known uniaxial and multiaxial failure stress states. The method processes all available mechanical test results in terms of failure stress states as one batch of data. For parameter fitting it implements the Maximum Likelihood Method and controlled numerical sampling techniques. The present work introduces the theoretical background as well as investigates the effect of the selection of the underlying strength distribution function type. The biggest benefit of this approach is the simultaneous handling of all available test data as well as the generality in terms of assumed strength distribution function and failure model type. In addition, the automatic evaluation of the uncertainty of all strength parameters enables introduction of a safety factor quantification related to uncertainty in material properties as one of the main contributors to scatter sources. A local sensitivity-based stress-state determination process is also introduced to design a set of input failure stresses that guarantee the identifiability of all parameters thus, ensuring robustness of the fitted constants. The entire methodology is demonstrated through the example of the Tsai-Wu model by processing experimental data and by comparing the results against the literature.

1. Introduction

Fiber-reinforced polymer composites (FRPC) offer exceptional properties and the opportunity to achieve superior strength-to-weight ratio by wisely chosen ply arrangement thanks to the anisotropic nature of these multiphase materials. However, the uncertainty of various design parameters has led to the use of high safety factors in structural design [52,53] which is too conservative in many cases thereby the potential of these fibrous materials cannot be fully exploited [54]. Uncertainties derive from the stochastic nature of constituent's properties, variation of manufacturing parameters, manufacturing defects [55], material testing [56], or failure under multiaxial loading [57] as well as uncertainty about the actual loading conditions acting on the component. Another issue related to the high level of uncertainty is the lack of robust fitting methods being able to handle sufficiently the high scatter in experimental data [56,59] as well as the lack of knowledge about the contribution of the individual tests to the identifiability of failure model parameters [58].

* Corresponding author at: eCon Engineering Kft., Kondorosi str. 3, H-1116 Budapest, Hungary.
E-mail address: laszlo.kovacs@econengineering.com (L. Kovács).

https://doi.org/10.1016/j.engfailanal.2023.107834
Received 27 September 2023; Received in revised form 6 November 2023; Accepted 26 November 2023
Available online 30 November 2023

To achieve high reliability and maximize the performance of FRPCs structures stochastic modeling and failure analysis are needed to be carried out. Soares [1], Sriramula and Chryssanthopoulos [2], and Chiachio et al. [3] summarised the existing approaches to assess the reliability of FRPC structures. Depending on the aim to the analysis, stochastic modeling can be performed at the micro-scale (constituent level) [4–8], mesoscale (ply/lamina level) [9–13], or macro-scale (laminate/structural level) [14]. To assess the reliability of composite materials, various methods are available: analytical predictions [15], probability integration methods e.g. first-order or second-order reliability method (FORM and SORM) [16,17], Monte Carlo Simulation (MCS) [16–20], stochastic finite element analysis (SFEA) [9–11,14,19] or the combination of these methods. While the random (Monte Carlo) sampling method requires a high number of simulations to produce high reliability, numerous solutions offer more efficient approaches e.g. Latin Hypercube Sampling [21,22] or Markov Chain Monte Carlo Sampling [23] method. Whichever stochastic approach is selected to infer the behavior or the properties of the system, those parameter identification techniques are usually driven by an iterative optimization process. In design optimization, various algorithms are used to find the most probable response of the material from a strength and/or deformation point of view even under multiaxial conditions. The application of the gradient method is one of the most common optimization strategies, however, it is sensitive to local min/max values. Evolutionary optimization methods, such as genetic algorithms (GA) [24–28] provide more accurate results but the application of these population-based strategies requires large computational effort. In recent years, more efficient optimzation techniques like artificial neural networks (ANN) [29,30] and Particle Swarm Optimization (PSO) method [31,32] emerged.

Another fundamental contributor to the successful and accurate failure model fit is the existence of an informative test data set. Different mechanical experiments contribute differently to the identifiability of failure model constants. It is vital to find a method that quantifies how much information the individual experiments possess with regard to the failure envelope parameters [44]. Extensive research is available in this subject related to the F_{12}^* fitting parameter of the Tsai-Wu model. Numerous researchers attempted to provide a deterministic, continuum-mechanics-based solution for this constant, such as Li et al [45,47] or Deteresa and Larsen [46]. However, there are very limited papers available where the identifiability of this parameter is analyzed against the uncertainty about either the available test data or the other in-plane strength parameters feeding the analytical evaluation [48].

It follows from the review above that in the topic of modeling failure behavior of FRPCs the focus is on establishing custom models that describe better first-ply failure than the well-known conventional ones. This is in many cases extended by a stochastic view where the strength components are approximated by a preselected probability distribution [20]. The micromechanics-based approaches are often compared against the conventional simple multiaxial ply-level models for validation purposes [60,61]. The approaches interpreted on ply level may be combined with an anisotropic constitutive model to handle simultaneously deformation behavior for more accurate operating stress and strain as well as failure state prediction. This allows the including of other phenomena such as viscoelasticity, viscoplasticity, creep, progressive degradation, etc. [62].

Regardless of the presented failure prediction techniques the accuracy in real multiaxial loading cases remains questionable. The main reason for that is the lack of representative experimental inputs available to cover such cases and therefore in the majority of such attempts, only numerical predictions are available based on Finite Element simulations. In addition, the stochastic nature of strength

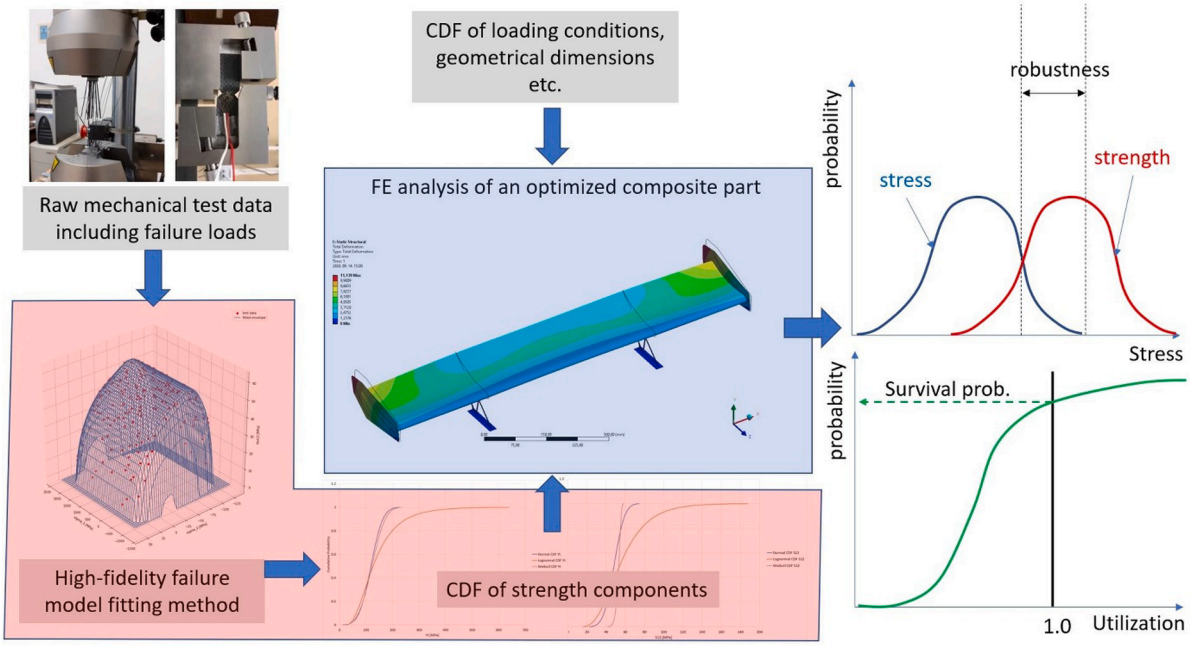

Fig. 1. Generic process flowchart of composite part integrity analysis combined with robustness check with the aid of High-Fidelity failure model fitting and FEA.

data is evaluated separately purely based on uniaxial experiments but it is not known how the level of uncertainty changes in multiaxial scenarios. Thus, for real industrial applications, an approach is necessitated that: represents well uniaxial and multiaxial failure, and can robustly fit the parameters and the uncertainty of a preselected failure and constitutive deformation model to all available conventional and unique experimental results in one go. In addition, the desired approach has the toolset to analyze the mechanical test results from the parameter-identifiability aspect.

The approach introduced in this paper offers a high-fidelity methodology to predict the first-ply failure of a composite structure under multiaxial loading. With the aid of this method, it is possible to establish material safety factors as a function of the predefined probability of survival which can be a way to clarify the relationship between risk of failure and weight of the part. A local sensitivity-based methodology is also provided to quantify the contribution of individual measurement results to the identifiability of the entire failure model. This approach helps construct the necessary mechanical experiments more consciously maximizing the information content with minimum testing effort.

This approach offers a toolset to quantify one major uncertainty source of the behavior of FRPCs: the variation of strength components. With this toolset, a more reliable robustness check can be performed on a composite design using Finite Element Analysis (FEA) since it delivers a precise assumption of the Cumulative Probability Distribution Function (CDF) of the strength components. The way this approach could be integrated into a FRPC part robustness analysis is provided in Fig. 1. The building block with a red background corresponds to the methodology to be described here.

2. The probabilistic failure model fitting approach

In this section theoretical background is provided about the FRPC first-ply failure models in general with a special focus on the one (Tsai-Wu) used to validate the fitting approach. In addition, the fitting process is described focusing on the entire workflow and the key elements of that: probabilistic objective function and the numerical sampling process to find failure probabilities. Finally, the practical implementation is discussed.

2.1. Overview of the most common first-ply failure models

In the past decades, many failure criteria have been developed to forecast the failure of a FRPC lamina in a multiaxial stress state. The simplest criteria are the maximum stress and maximum strain criteria, which handle each stress/strain component independently. The interactive failure criteria, such as Tsai-Wu [33], Tsai-Hill, and Hoffman [34] criteria, use a quadratic equation to predict lamina failure in which the stress components act together. The drawback of these criteria is that they do not provide information about the failure mode. The advanced failure criteria [35–39] are physically based criteria that not only consider the influence of each stress component on each other but also separate fiber dominated failure and inter-fiber failure (matrix and interfacial failure). The composite community made efforts [40–43] to establish a failure criterion that predicts the failure accurately, but no superior criterion has

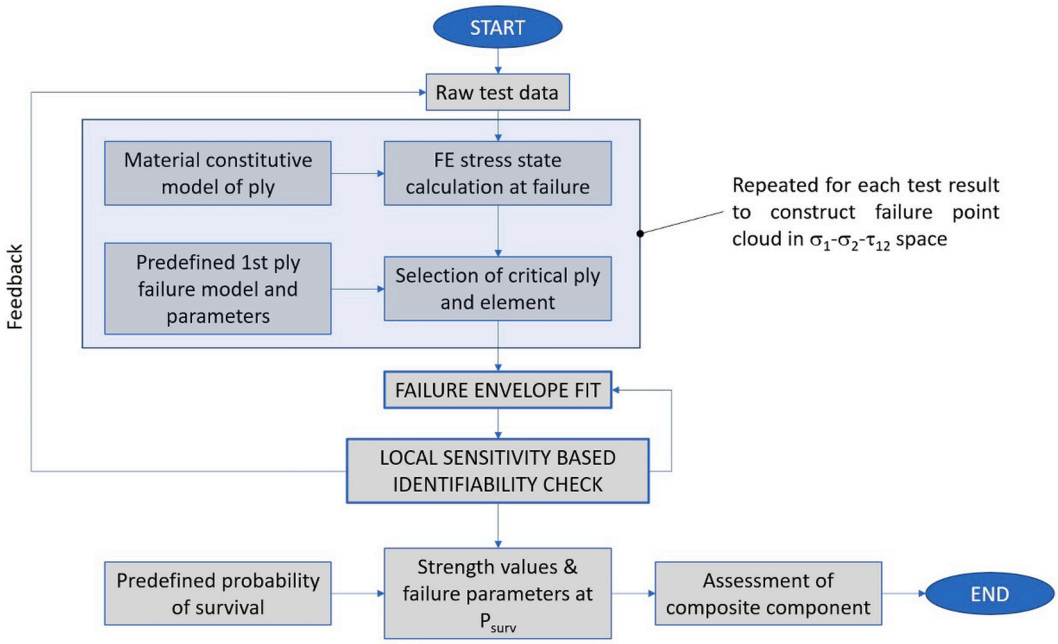

Fig. 2. Flowchart of holistic first-ply failure model parameter fitting workflow and integration of that in sophisticated FRPC component FE assessment.

been found so far. In this paper, a widespread criterion is introduced, namely the Tsai-Wu, which has been used as limit state equations in the present method.

The Tsai-Wu criterion is based on the von Mises theory and can be expressed in the following form [33]:

$$\frac{\sigma_{11}^2}{X_t \cdot X_c} + \frac{\sigma_{22}^2}{Y_t \cdot Y_c} + \frac{2 \cdot F_{12}^* \cdot \sigma_{11} \cdot \sigma_{22}}{\sqrt{(X_t \cdot X_c \cdot Y_t \cdot Y_c)}} + \left(\frac{1}{X_t} - \frac{1}{X_c}\right) \cdot \sigma_{11} + \left(\frac{1}{Y_t} - \frac{1}{Y_c}\right) \cdot \sigma_{22} + \frac{\tau_{12}^2}{S_{12}^2} = \mathrm{IRF} = 1 \quad (1)$$

where σ_{11} is the fiber direction stress component, X_t is the fiber direction tensile strength, X_c is the fiber direction compressive strength, σ_{22} is the transverse normal stress component, Y_t is the transverse tensile strength, Y_c is the transverse compressive strength, τ_{12} is the in-plane shear stress component, S_{12} is the in-plane shear strength and F_{12}^* is the Tsai-Wu constant. The so-called Inverse Reserve Factor (IRF) expresses the utilization of the material at the given stress state. Taking a value less than 1.0 refers to a safe state. Once IRF takes a value of 1.0 the onset of failure is expected.

2.2. Overview of the elaborated holistic first-ply failure model fitting workflow

The main steps of the workflow elaborated to provide a better quality and high-fidelity fit of FRPC ply strength values and failure parameters are detailed here. The scope of this paper is to introduce the statistical parameter fitting concept and to prove its advantages therefore all the other steps listed in this section are briefly summarized.

The entire workflow is described by the flowchart shown in Fig. 2. The description of the main steps is as follows. Firstly, the raw test data is generated by conducting a variety of mechanical experiments on FRPC samples. This should include the specimen dimensions and layup sequence as well as failure loads. Applying the failure loads on the virtual (FE) model of the specimens the actual stress state in each ply and element can be reliably estimated. A very important prerequisite for this step is to have a precise ply-specific orthotropic material constitutive model that is the same as the one implemented in the FE analyses of the final product. The engineering constants of that model can be fitted based on the recorded load-deformation curves from appropriate tests. The evaluation of the material constitutive model and the FE modeling approach is out of the scope of this paper.

For each virtual specimen model, the failed layer and location of failure shall be found which can be based on the aforementioned FE models' stress results in each layer. The element/layer providing the largest IRF with a preselected nominal failure envelope is selected for further evaluation. This means the three in-plane stress components (σ_1, σ_2, τ_{12}) are extracted and stored. Repeating the critical stress calculation steps for each available experiment a database is created which stores the three in-plane stress components at failure at the critical element/layer for all test pieces. This database forms a cluster of data points in the coordinate system of σ_1-σ_2-τ_{12} stresses. The next step is to perform the high-fidelity fit of the failure envelope to these data points. Since this paper mainly focuses on this method it is detailed further in Section 2.3. The outcome of this step is a set of strength CDF parameters that determine the likely interval for the strength component in question as well as additional first-ply failure model-specific fitting parameters for the selected theoretical failure approach.

Before proceeding to the FE analysis of the composite component it is also quantified if the constants of the first-ply failure models can be evaluated from the available set of test results. For this, a local sensitivity-based evaluation is conducted that connects the level of identifiability of a parameter with the actual failure stress state of the experiment. In case of a not identifiable parameter, a suitable experiment can be analytically designed using standard test setups and unidirectional (UD) ply orientation based on continuum-mechanical principles. This method is introduced in Section 2.5 and demonstrated on a real experimental dataset in Section 3.4.

For practical use of the selected first-ply failure model a preferred probability of survival value (P_{surv}) can be defined as input. There is a one-to-one relationship between the probability of survival value and the corresponding strength which is described by the actual fitted CDF. Thus, using the predefined probability the corresponding strength values can be calculated that will serve as input for the upcoming FE analysis of the FRPC part. This way the compliance of the part can be associated with a certain risk of failure (1-P_{surv}) which leads to more sophisticated structural assessments. In addition, the fitted CDF of each strength component can serve as an important input for component robustness analysis (Fig. 1).

2.3. Probabilistic failure envelope fitting approach – objective function

In the newly introduced probabilistic approach, the objective function computes the aggregate probability of failure including all test data. This objective function implies how likely is that the tested specimens at the measured stress states fail at the given set of CDF of the strength components. The general mathematical expression of the maximum likelihood estimation (MLE) concept is as follows [63]:

$$OF_{ML} = \prod_{i=1}^{N} P_i \cdot \prod_{j=1}^{M} (1 - P_j) \quad (2)$$

where OF_{ML} stands for the objective function to maximize, N is the number of failed tests, M is number of unfailed tests at the maximum recorded load level, P_i stands for the probability to fail of the "i-th" broken specimen at the measured stress level and with the assumed strength CDFs and failure parameters, and P_j means the probability of failure of the "j-th" unbroken specimen at the measured stress level and below and with the assumed strength CDFs and failure parameters.

Based on the general definitions of Probability Density Function (PDF) and CDF in statistics, one can say that assuming continuous

probability distribution for ply strength P_i can be evaluated using the PDF and P_j comes from the CDF functions of the strength component.

The objective is to maximize OF_{ML}, however, the numerical optimizers are more robust in minimum search, thus, the target of optimization in this case can be expressed in the following form:

$$(OF_{ML})^{-1} = min \tag{3}$$

During minimum search, the parameters defining CDF of all 5 strength components and additional first-ply failure model-specific constants are being sought.

The main assumptions used to implement the MLE concept in the failure model fitting workflow are the following. Because P_i is a 5-dimensional function of the strength CDFs as well as it is not clear if those CDFs are independent or not it was decided to implement a numerical estimation of the failure probability using a controlled sampling method. The term with P_j in Equation (2) was disregarded because it was deemed to be an unrealistic scenario to cease a quasi-static tensile test before failure if the aim is to get information about strength. The five strength values (X_t, X_c, Y_t, Y_c, and S) were assumed to follow a certain CDF. Any other first-ply failure-specific fitting constants were assumed to be a constant value instead of a probabilistic variable. For instance, in the case of the Tsai-Wu model the F_{12}* parameter is the failure-specific fitting constant.

The mathematical apparatus to implement the MLE method is somewhat more complex than what is needed for a conventional Least Squares Method based objective function (error minimization), and the number of parameters to optimize is higher as well, however, there are several advantages that prove that this procedure is the better choice. The CDFs due to their mathematical formulation result in an inherent weighting of data points. Therefore, this method is not as sensitive to outlier data points as the Least Squares Method. The outcome of the fitting exercise is the Probability Distribution Function of each strength component that makes it possible to specify probability level-dependent safety factors.

The fitter was built in a modular way which allows the implementation of arbitrary distribution function types describing the variation in strength components. The selected CDF is used to evaluate the probability of failure of each test data and is calculated by a numerical approximation. At the actual state of optimization for each test result the assumed CDFs are sampled several times and it is checked how many times out of the total number of scenarios the calculated IRF falls into the vicinity of 1.0. This gives an estimated P_i for each specimen. The objective function of the MLE optimization will then be the product of the individual failure probabilities. This is being attempted to maximize by the optimizer whilst tuning the failure model constants and strength CDF parameters (see Fig. 4). Due to the five independent strength CDFs to be considered simultaneously during sampling the only computationally effective option was to implement a multidimensional controlled sampling method. Thus, the Latin Hypercube Sampling (LHS) [21,22] approach was introduced. In the implemented LHS method the generated sample size was 500 per test result in each optimization round with regards to the strength CDFs and failure parameters.

Currently, three different CDF types are available in the fitter: Normal (Gaussian), Lognormal, and Weibull CDFs. The reasoning behind using these three types is as follows: Gaussian distribution is usually the default option in Engineering disciplines when it comes to describing the uncertainty of any measured parameter, especially strength. It describes the real variation well if the scatter is moderate (CoV $<$ 20 %). However, in cases when the scatter is large and it is not well justified that the distribution of the individual strength components is symmetric and has similar characteristics, using an asymmetric distribution provides a more flexible solution. By changing the parameters of an asymmetric CDF, the shape of the PDF can vary quite flexibly. This is especially true for Weibull distribution which can cover symmetric and significantly skewed CDF as well. The lognormal distribution is the right choice if the variable in question can occur in a wide interval even spreading over a few orders of magnitudes. The effect of the CDF selection was also investigated as part of the present work in Section 3.2.

After identifying the CDF parameters, any strength component corresponding to a certain level of probability of survival can be calculated with the following formulas [64]:

$$[X(P_{surv})]_{normal} = \overline{X} \cdot (1 - z \cdot CoV_X) \tag{4}$$

$$[X(P_{surv})]_{lognorm} = \frac{\overline{X}}{e^{z \cdot \sigma_{lognorm}}} \tag{5}$$

$$[X(P_{surv})]_{Weibull} = \lambda \cdot [-ln(P_{surv})]^{\frac{1}{k}} \tag{6}$$

where P_{surv} is the probability to survive, $\overline{X}$ corresponds to the median of fitted strength, CoV_X denotes the coefficient of variation of fitted strength (for Normal and Lognormal distributions), λ is the scale parameter, k refers to the shape parameter of Weibull distribution. The parameter "z" means the "number of sigmas" which can be evaluated with the inverse CDF of X [64]:

$$z = CDF^{-1}_{STDNORM}(P_{surv}) \tag{7}$$

where $CDF^{-1}_{STDNORM}$ refers to the formal notation of the inverse standard normal distribution function (with the probability level in brackets as the argument of it).

2.4. Coding and implementation

The High-fidelity method for strength evaluation has been coded in the form of an automated workflow. The implemented MLE and controlled sampling-based parameter fitter is graphically represented in Fig. 4. It consists of two loops embedded into each other. The outer loop is controlled by the parameter optimizer. This varies the fitting parameters (strength CDF parameters as well as the additional failure model-specific constants) depending on the actual value of the total probability as the objective function. Within each optimization round the code builds up the objective function sequentially. It calculates the probability of failure for each test data at the actual CDFs and fitting parameters as described in Section 2.2 and multiplies the individual "P_i" probabilities. Once the last data point is processed, the objective function value is sent back to the outer loop for the optimizer to decide how to adjust the fitting parameters. The selected optimization algorithm governing the fitting parameter adjustments was a genetic algorithm (GA). In addition, the code computes the actual values of the fitted parameters at the predefined probability of survival using the optimized strength CDFs with Equations (4), (5) or (6) depending on the selection of the underlying strength CDF type. To help understand the fitting quality, each envelope is also graphically highlighted against the raw test data in the in-plane stress space. One example of that is shown in Fig. 3. Finally, the fitted failure model is put through a parameter identifiability analysis and if there are any constants that turn out to be unidentifiable, an alternative test setup is suggested to provide an informative stress state for the unidentifiable model constants as per Section 2.5.

2.5. Design of experiments based on local parameter sensitivity

To check the robustness of the fitted failure model, it has to be investigated if the available failure stress states have any influence on the parameters of it. For that, we defined a measure called local sensitivity as the local partial derivative of the failure model:

$$s_{\theta i}([\sigma_{11}, \sigma_{22}, \tau_{12}]) = \left| \frac{\partial f([\sigma_{11}, \sigma_{22}, \tau_{12}], [\theta])}{\partial \theta i} \right| \tag{8}$$

Where $s_{\Theta i}$ denotes local sensitivity depending on the [σ_{11}, σ_{22}, τ_{12}] failure stress state, f represents the IRF of the selected failure model being dependent on the failure stress state, and the model constants collected in the vector [Θ], Θ_i represents one fitting constant of f.

The higher $s_{\Theta i}$ gets the more information is stored about Θ_i parameter at the [σ_{11}, σ_{22}, τ_{12}] failure stress state. It also follows from this definition that if the available set of failure stress states gives nearly zero local sensitivity for a certain fitting parameter, that parameter does not have an influence on the IRF value at those loading conditions, therefore it cannot be reliably derived from them regardless of the parameter evaluation method. In these scenarios, another mechanical experiment has to be designed providing a failure stress state with adequate $s_{\Theta i}$.

The local sensitivity values as a function of failure model fitting constants and stress state for the Tsai-Wu model which is the focus of this paper are as follows:

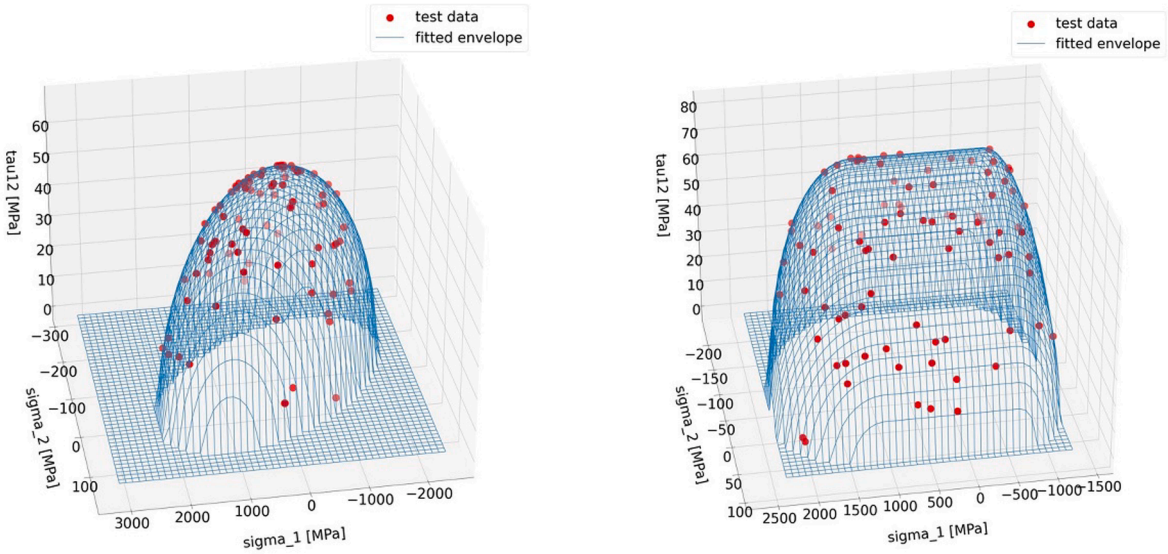

Fig. 3. Graphical representation of fitted failure envelope in the coordinate system of in-plane ply stress components against raw test data using Tsai-Wu (left) and Puck (right) criteria.

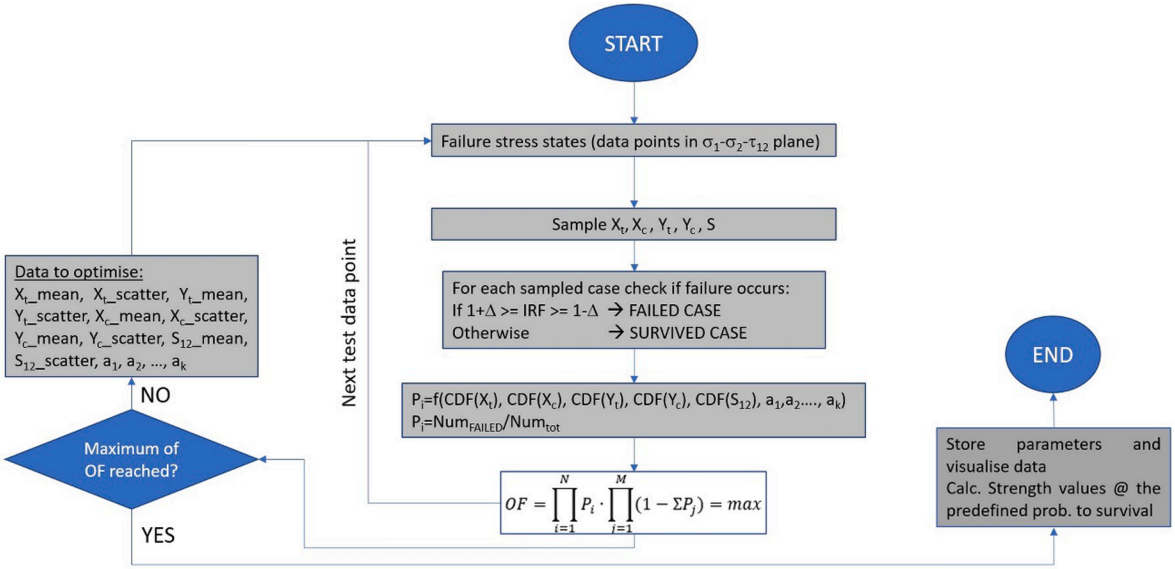

Fig. 4. Flowchart about the implementation of the failure envelope parameter fitting methodology used in the holistic first-ply failure model fitting workflow.

$$\left|\frac{\partial f_{TW}}{\partial Xt}\right| = \left| -\sigma_{11} \cdot \left[\frac{\sigma_{11}}{X_c} \cdot \frac{1}{X_t^2} + \frac{1}{X_t^2} + \frac{F_{12}^* \cdot \sigma_{22}}{\sqrt{X_c \cdot Y_t \cdot Y_c}} \cdot \frac{1}{X_t^{1.5}}\right] \right| \tag{9}$$

$$\left|\frac{\partial f_{TW}}{\partial Xc}\right| = \left| -\sigma_{11} \cdot \left[\frac{\sigma_{11}}{X_t} \cdot \frac{1}{X_c^2} - \frac{1}{X_c^2} + \frac{F_{12}^* \cdot \sigma_{22}}{\sqrt{X_t \cdot Y_t \cdot Y_c}} \cdot \frac{1}{X_c^{1.5}}\right] \right| \tag{10}$$

$$\left|\frac{\partial f_{TW}}{\partial Yt}\right| = \left| -\sigma_{22} \cdot \left[\frac{\sigma_{22}}{Y_c} \cdot \frac{1}{Y_t^2} + \frac{1}{Y_t^2} + \frac{F_{12}^* \cdot \sigma_{11}}{\sqrt{X_t \cdot X_c \cdot Y_c}} \cdot \frac{1}{Y_t^{1.5}}\right] \right| \tag{11}$$

$$\left|\frac{\partial f_{TW}}{\partial Yc}\right| = \left| -\sigma_{22} \cdot \left[\frac{\sigma_{22}}{Y_t} \cdot \frac{1}{Y_c^2} - \frac{1}{Y_c^2} + \frac{F_{12}^* \cdot \sigma_{11}}{\sqrt{X_t \cdot X_c \cdot Y_t}} \cdot \frac{1}{Y_c^{1.5}}\right] \right| \tag{12}$$

$$\left|\frac{\partial f_{TW}}{\partial S12}\right| = \frac{2 \cdot \tau_{12}^2}{S_{12}^3} \tag{13}$$

$$\left|\frac{\partial f_{TW}}{\partial F_{12}^*}\right| = \left|\frac{2\sigma_{11} \cdot \sigma_{22}}{\sqrt{X_t \cdot X_c \cdot Y_t \cdot Y_c}}\right| \tag{14}$$

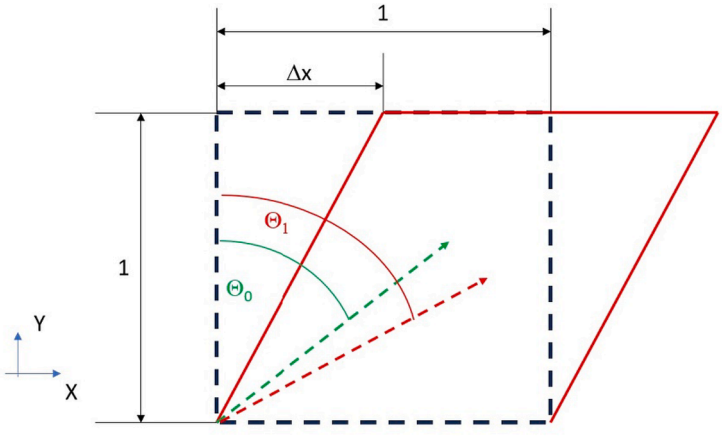

$$\Theta_1 - \Theta_0 = \frac{arctan(\Delta x)}{2}$$

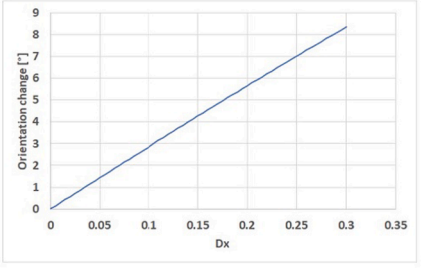

Fig. 5. Schematic description of simple shear deformation of a unit-square shaped composite plate with Θ_0 initial and Θ_1 draped fiber orientation.

In case any of the fitted parameters turns out to have nearly zero sensitivity at the available failure stress states, an analytical method is suggested to find the most informative conventional test setup concept and UD ply orientation. This Design of Experiment (DoE) method is suitable for conventional mechanical experiments such as uniaxial tension/compression, simple shear or pure shear. The kinematics of such tests can be easily described with the toolset of continuum mechanics. In addition, the approach suggested here assumes that the FRPC laminates sent to test are UDs, follow an either linear or nonlinear orthotropic constitutive model and the stress distribution of them is uniform. This is not true in reality due to the local stiffening effects of boundary conditions, however, that can be investigated in detail with numerical simulation. This method can be used for conceptual design which determines the baseline for a detailed fixture design if needed including the treatment of local stress concentration or hazard of buckling.

Once the conventional test kinematics is selected, the corresponding deformation gradient tensor in a predefined global coordinate system – usually aligned with the main loading direction – is known from the literature. As an example, for the simple shear experiment, in a global coordinate system as shown in Fig. 5 the deformation gradient tensor $\mathbf{F}_{ss}$ is as follows [65].

$$\boldsymbol{F}_{ss} = \begin{bmatrix} 1 & \Delta x & 0 \\ 0 & 1 & 0 \\ 0 & 0 & 1 \end{bmatrix} \tag{15}$$

From that, the right Cauchy-Green deformation tensor (**C**) can be calculated with the following formula [49].

$$\boldsymbol{C} = \boldsymbol{F} \cdot \boldsymbol{F}^T \tag{16}$$

As next, the Green-Lagrange strain tensor in global coordinate system can be calculated as follows [49].

$$\boldsymbol{E} = \frac{1}{2}(\boldsymbol{C} - \boldsymbol{I}) \tag{17}$$

Where **I** denotes the identity matrix.
For the previously introduced simple shear example, the Green-Lagrange strain tensor looks like this.

$$\boldsymbol{E}_{ss} = \begin{bmatrix} 0 & \frac{\Delta x}{2} & 0 \\ \frac{\Delta x}{2} & \frac{\Delta x^2}{2} & 0 \\ 0 & 0 & 0 \end{bmatrix} \tag{18}$$

In continuum-mechanics finite strain theory typically orthotropic material models are interpreted as the relationship between the Green-Lagrange strain tensor and the 2nd Piola-Kirchhoff stress tensor. The 2nd Piola-Kirchhoff stress vector in the global coordinate system can be calculated with a general Hook's law using the Voigt notation [51].

$$\boldsymbol{S} = \boldsymbol{C} \cdot \boldsymbol{E} = \boldsymbol{T}^{t}\boldsymbol{C}_{l}\boldsymbol{T} \cdot \boldsymbol{E} \tag{19}$$

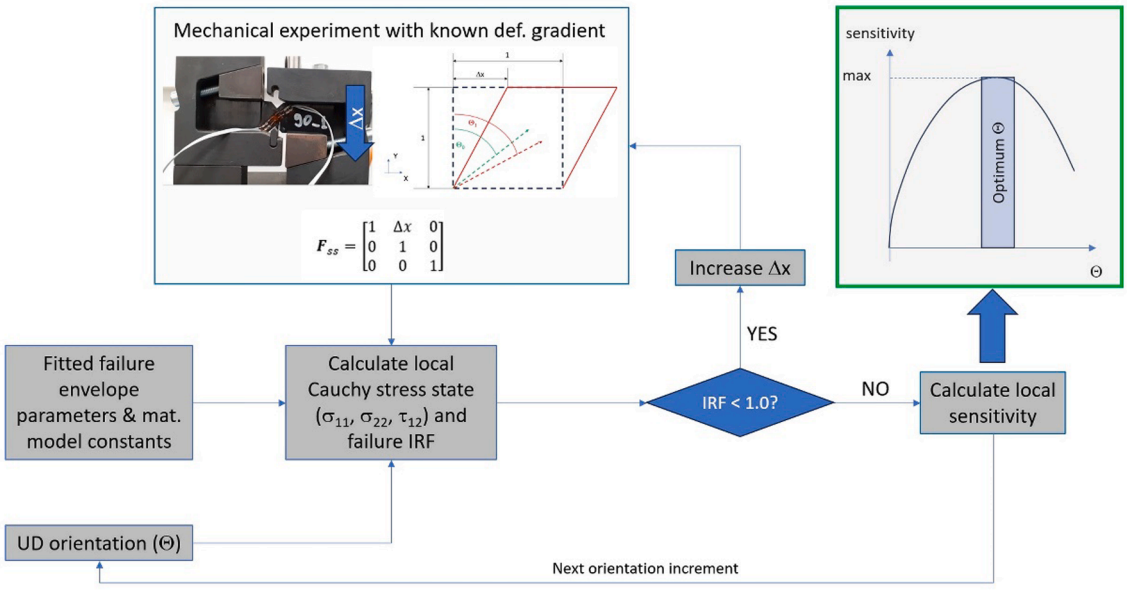

Fig. 6. Schematic flowchart of the iterative Design of Experiments technique for the evaluation of the most informative fiber orientation through the example of a simple shear experiment.

Where **C** denotes the orthotropic tangent or chord compliance matrix in the global coordinate system, $\mathbf{C_l}$ represents the same compliance matrix in the local material coordinate system and **T** corresponds to the rotation transformation matrix as per Cook [50].

For a general orthotropic ply, the local $\mathbf{C_l}$ matrix is to be calculated as follows [51].

$$\boldsymbol{C}_l = \begin{bmatrix} \frac{1}{E_{11}} & \frac{-\nu_{21}}{E_{22}} & \frac{-\nu_{31}}{E_{33}} & 0 & 0 & 0 \\ \frac{-\nu_{12}}{E_{11}} & \frac{1}{E_{22}} & \frac{-\nu_{32}}{E_{33}} & 0 & 0 & 0 \\ \frac{-\nu_{13}}{E_{11}} & \frac{-\nu_{23}}{E_{22}} & \frac{1}{E_{33}} & 0 & 0 & 0 \\ 0 & 0 & 0 & \frac{1}{G_{12}} & 0 & 0 \\ 0 & 0 & 0 & 0 & \frac{1}{G_{23}} & 0 \\ 0 & 0 & 0 & 0 & 0 & \frac{1}{G_{13}} \end{bmatrix}^{-1} \tag{20}$$

Where E_{11} stands for the normal in-plane modulus in fiber direction, E_{22} represents the in-plane transverse modulus, E_{33} is the modulus normal to the plane of the ply, G_{12} is the in-plane shear modulus, G_{23} and G_{13} represent the interlaminar shear moduli and ν_{12}, ν_{21} are the in-plane major and minor Poisson's ratios and the ν_{13}, ν_{31}, ν_{23}, ν_{32} pertain to the interlaminar major and minor Poisson's ratios.

In terms of failure, the real acting stresses are relevant in each ply. In finite strain theory this is equivalent to the true (Cauchy) stress tensor that can be evaluated from the 2nd Piola-Kirchhoff stress tensor with the following formula [49].

$$\boldsymbol{\sigma} = J^{-1} \cdot \boldsymbol{F} \cdot \boldsymbol{S} \cdot \boldsymbol{F}^{\boldsymbol{T}} \tag{21}$$

Where J denotes the determinant of the deformation gradient tensor (Jacobian). This parameter represents the volumetric deformation. In the simple shear example, no volumetric deformation takes place, thus, J = 1.

$$\boldsymbol{\sigma}_{ss} = \boldsymbol{F}_{ss} \cdot \boldsymbol{S} \cdot \boldsymbol{F}^{\boldsymbol{T}}{}_{ss} \tag{22}$$

The Cauchy stress tensor obtained this way is interpreted in the global coordinate system. But, for the local sensitivity calculation, the local stress tensor has to be known in a coordinate system aligned with the fiber orientation. This local stress tensor can be evaluated from σ with a simple tensor rotation transformation around the "Z" axis that represents the layer's out-of-plane direction [50].

$$\boldsymbol{\sigma}_l = \begin{bmatrix} \cos\theta & -\sin\theta & 0 \\ \sin\theta & \cos\theta & 0 \\ 0 & 0 & 1 \end{bmatrix} \cdot \boldsymbol{\sigma} \cdot \begin{bmatrix} \cos\theta & -\sin\theta & 0 \\ \sin\theta & \cos\theta & 0 \\ 0 & 0 & 1 \end{bmatrix}^{T} \tag{23}$$

Where Θ represents the fiber orientation compared to the global X axis.

With the formulas above the local stresses feeding the sensitivity calculation can be analytically predicted for a known standard mechanical test kinematics (deformation gradient tensor) and UD tape orientation. This allows for building an automated method that finds the failure stress state and the corresponding local sensitivity for a given test setup as a function of the UD orientation as shown in Fig. 6. With the aid of this analytical technique, one can get a quick estimate about the UD orientation needed for a certain test setup that produces the highest local sensitivity and therefore the most information about a certain failure model parameter being attempted to fit robustly. This method is also demonstrated via real mechanical experiments in Section 3.4.

3. Experimental validation of the fitting and DoE method

To demonstrate the viability of the presented failure model fitting process numerous simple mechanical experiments were conducted on flat UD samples of a preselected FRPC ply material. The selected material type was *Toray Cetex® TC1225 - Standard Modulus Carbon 145gsm UD Tape 34 % RC*. The main properties of the selected CFRP are collected in Table 1.

Numerous mechanical experiments were conducted as per relevant standards that were used for several purposes such as the derivation of nonlinear orthotropic constitutive model of the ply for FE simulation, calculation of nonlinear failure stress states of each test piece as well as fitting a Tsai-Wu failure envelope to the available experimental failure stress states with the MLE-based fitting method. The details of the conducted experiments are collected in Table 2.

The test setup for uniaxial tension and uniaxial compression is shown in Fig. 7. An example of flexure and V-notched beam shear testing is highlighted in Fig. 8. All experiments were conducted up to specimen failure to have information about failure loads and thus, have the opportunity to infer the complex failure stress states of each test piece with the aid of FE simulation.

3.1. Derivation of failure stress states

As per Fig. 2 evaluation of composite UD ply mechanical properties was the first step to calculate the failure stress state of each specimen. This was done with the aid of virtual representations of the conducted tests in the form of adequate FE models. The main

features of the used FE models were as follows:

- LS-DYNA implicit solver,
- 8-node quadratic fully integrated brick elements (ELFORM = 2),
- Nonlinear orthotropic material model used (MAT040) with input stress–strain curves defined in normal and shear directions (separate data in compression and tension),
- Assumed ply constitutive model: transversely isotropic ($E_{22} = E_{33}$, $G_{12} = G_{13}$ and $\nu_{21} = \nu_{31}$). This is a special form of orthotropic behavior in interlaminar planes, however, in the plane of the ply the material follows an orthotropic constitutive law.
- Material coordinate system of each element adjusted to the target fiber direction.

The required material properties (stress–strain curves and Poisson's ratios) were evaluated from specific experiments listed in Table 2. These experiments with the relevant stress–strain curves and initial moduli derived from them are given in Table 3.

An example of a meshed model for flexure showing the axial stress distribution and deformed shape in the loaded condition is shown in Fig. 9. Each test type had a corresponding simulation associated with it. From the simulations, the relationship between external loading and internal in-plane stresses could be established. Since the failure load for all experiments was recorded, the pertaining stress state was interpolated from the aforementioned load vs. stress data. These σ_{11}- σ_{22}– τ_{12} stress states were directly input into the MLE based failure envelope fitter.

3.2. Results of failure envelope fit to experimental results

The MLE based Tsai-Wu failure envelope fit simultaneously provided all parameters. The detailed results are highlighted in Table 4 both for two different fitting scenarios. In scenario 1 the assumed underlying strength distribution function was normal, whilst in the 2nd case a two-parameter Weibull distribution was used. It follows clearly from the figures that in terms of the strength value medians both assumed distributions provided a very close answer that implies the robustness of the fitting technique as well as the appropriateness of the distribution functions. The coefficient of variation (CoV) of the strength components calculated for Gaussian distribution falls into the region of 13–23 % which was expected due to the apparent noise in the experimental data. The only outlier from this aspect is the strength in fiber direction (X_c) with 34 % CoV. This might imply that either the Tsai-Wu is not the most suitable failure model based on the available test dataset or that a skewed CDF describing the uncertainty about that parameter would be a better choice (like Weibull). The quality of the fit was described by the Total Likelihood Estimator (TLE). Based on that the quality of the two fits was very similar. The TLE is a quantity proportional to the MLE objective function as per Equation (2) but it is more efficient from a computational aspect:

$$\mathrm{TLE} = -\sum_{i=1}^{N} log(P_i) \tag{24}$$

As a graphical representation of the fitted envelopes, Fig. 10 shows their projection on the σ_{11}- σ_{22} plane along with the test results with nearly zero shear stress. Fig. 11 highlights the fitted envelopes along with all available test data in the σ_{11}- σ_{22}– τ_{12} space. The fitted strength CDFs are presented in Fig. 12. In general, it can be stated that a skewed CDF with a broader left tail described better the strength distributions than the symmetric Gaussian distribution. The only exception is Y_t where the two CDFs turned out to be nearly identical.

As can be seen in Fig. 10 the fitted Tsai-Wu ellipses are quite different in shape although the fitted strengths (intersection points of envelope and stress axes) agree well. This is the effect of the dissimilar optimized F_{12}^* constants as shown in Table 4. A possible reason for such an inconsistent fit might be the lack of information content that the available experimental results have with regard to the F_{12}^* constant. If the failure surface is insensitive to the F_{12}^* constant at the available failure stress states, it cannot be fitted reliably. This was investigated with the local sensitivity-based technique detailed in Section 2.5. The conclusions are given in Section 3.4.

3.3. Results of local sensitivity-based identifiability check

To investigate if the available experiments have a strong enough correlation with the F_{12}^* parameter, the fitted failure surface in σ_{11}- σ_{22}– τ_{12} space was discretized by a mesh where the local sensitivity was calculated at each node. This is highlighted in Fig. 13. This mesh is projected on the σ_{11}- σ_{22} plane and the color of each node represents the level of sensitivity, i.e. the identifiability of F_{12}^*constant. The larger circle symbols in Fig. 13 represent the available experimental failure stress states also projected on the normal stress plane. It follows from this local sensitivity check that all data points fall into the nearly zero sensitivity region from the F_{12}^* aspect. The circled zone represents the stress states where the $F_{12}^*$is identifiable. Based on this investigation one can conclude that for a reliable fit of F_{12}^* tensile-compressive biaxial mechanical experiment is needed as far as the in-plane normal stresses are concerned.

Table 1
Properties of the FRPC laminate selected for method validation.

Resin type	Manufacturing method	Reinforcement	Fiber volume content	Layup sequence	Plate thickness
Thermoplastic (PAEK)	Hot pressing from organosheets	UD CF (145 gsm)	66 %	$[0]_8$	1.1 mm

Table 2
Details of performed validation experiments.

Experiment type	Standard	Fiber orientation	Number of test pieces	Mechanical test frame	Measured quantities
Uniaxial tension	ISO 527-5	0°	15	Instron® 8801 +/− 100 kN high-frequency servo-hydraulic machine	Load [N], strain [%]
Uniaxial tension	ISO 527-5	90°	15		
Uniaxial tension	ISO 527-5	15°-30°-45°	8-8-6		Load [N], extension [mm]
Uniaxial compression	ASTM D3410	0°-15°-30°-45°-90°	10-5-5-5-10	Zwick Z250 20kN servoelectric testing frame	Load [N], crosshead displacement [mm]
3-point-bending	ISO 14125	0° and 90°	10-10	Hegewald & Peschke +/− 50 kN servoelectric testing frame	Load [N], specimen deflection [mm]
4-point-bending	ISO 14125				
Iosipescu V-notched shear	ASTM D5379		5-5		Load [N], shear strain [%]

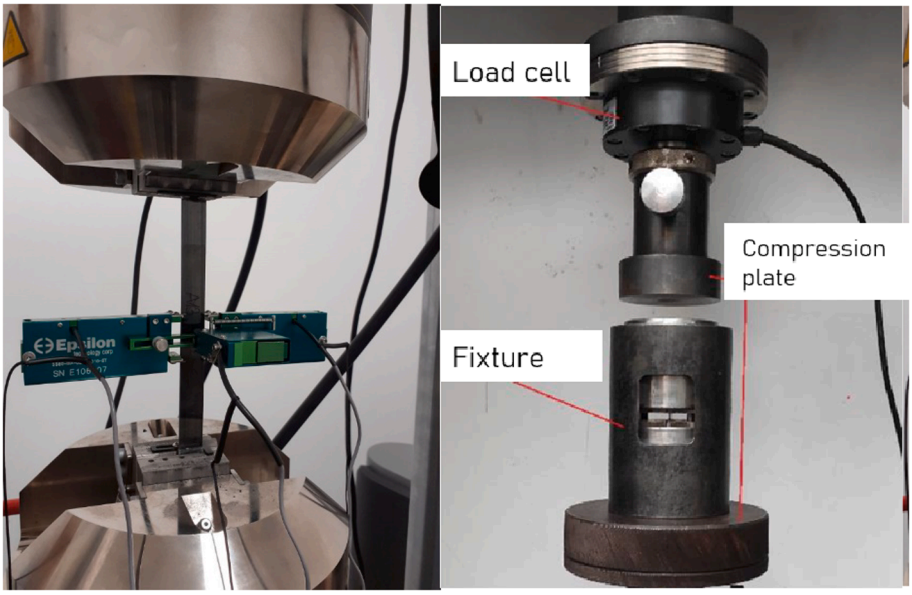

Fig. 7. Typical test setup for ISO 527-5 tensile (left) and ASTM D3410 compressive testing (right).

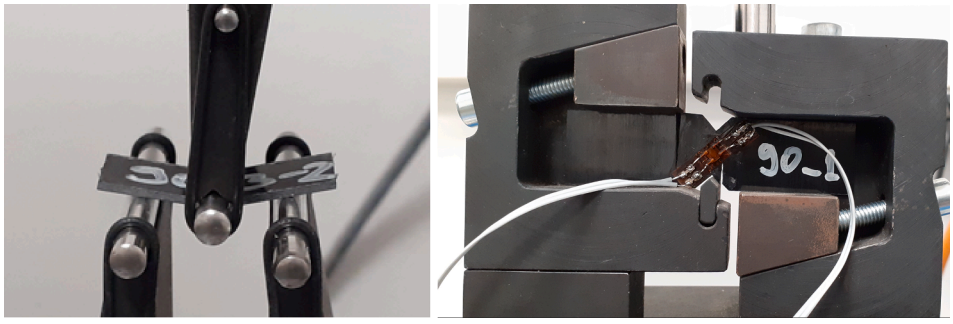

Fig. 8. Typical test setup for ISO 14125 flexural (left) and ASTM D5379 V-notched beam testing (right).

3.4. *Suggested experiment setup for reliable F_{12}*fit*

To find a suitable experiment for a successful F_{12}*fit, the analytical DoE concept was implemented as introduced in Section 2.5. In terms of the predefined kinematics, a simple shear experiment was chosen with a known deformation gradient tensor as shown in Section 2.5. The purpose of this investigation was to find the relationship between the ply orientation of the UD plate being simple shear tested and the F_{12}* identifiability. Once this relationship is known, one can choose the "most informative" UD orientation for the preselected test type. After conducting the calculation steps with the strength parameters from Gaussian CDF fit, the UD orientation vs. relative sensitivity graph was constructed as shown in Fig. 14. The actual UD orientation (denoted as Θ in Fig. 14) is measured from the

Table 3
Experimentally derived stiffness properties of the selected composite UD ply.

Experiment type	Fiber orientation	Derived stress–strain curve	Derived initial parameters	Material parameters evaluation process
Uniaxial tension	0°	σ_{11}- ε_{11} – tension*	$E_{11t} = 126$ GPa $\nu_{12} = 0.355$	From direct load and strain measurement as per standard
Uniaxial tension	90°	σ_{22}- ε_{22} – tension*	$E_{22t} = 8137$ MPa	
3-point-bending	0°	σ_{11}- ε_{11} – compression*	$E_{11c} = 124$ GPa	Indirect way via iterative calibration of the surrogate FE model's material card
4-point-bending	0°			
3-point-bending	90°	σ_{22}-ε_{22} – compression*	$E_{22c} = 2.5$ GPa	
4-point-bending	90°			
Uniaxial tension	15°-30°-45°	τ_{12}-γ_{12}	$G_{12} = 4282$ MPa	
Iosipescu V-notched shear	0° and 90°		$G_{12} = 4200$ MPa	From direct load and strain measurement as per standard

*Linear stress–strain relationship.

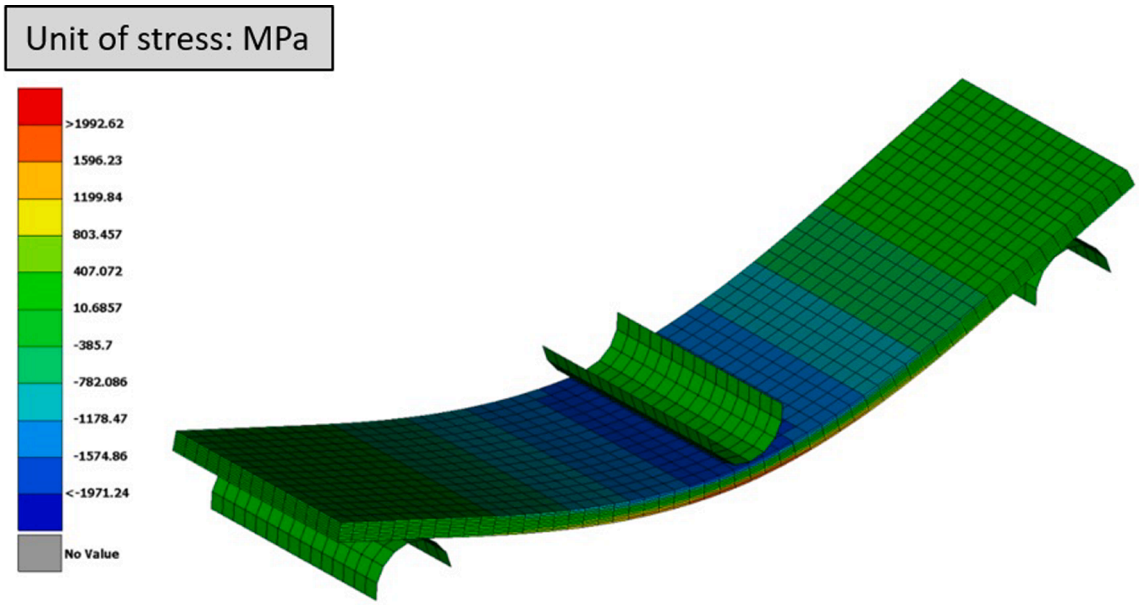

Fig. 9. FEA-based stress state prediction at failure, 3-point-flexure as per ISO 14125.

Table 4
Detailed results of the MLE based Tsai-Wu failure envelope fit.

Parameter	Normal CDF – TLE = 104			Weibull CDF – TLE = 101		
	Mean	CoV	Median	Scale factor (λ)	Shape parameter (k)	Median
X_t	2311	0.13	2311	2340	21.52	2301
X_c	735	0.35	735	728	15.22	711
Y_t	75	0.24	75	80	4.63	74
Y_c	199	0.14	199	217	21.84	213
S_{12}	66	0.19	66	65	3.06	58
F_{12}*	−0.0023	–	−0.0023	–	–	0.3024

side of the plate being perpendicular to the direction of shear. The relative sensitivity was calculated by normalizing the actual local sensitivity value with the maximum value obtained over the discretized stress points on the failure surface. It follows clearly from the figure that a UD orientation ranging between 40 and 70° results in the highest expected local sensitivity for a simple shear experiment which is still the ca. 20 % of the maximum achievable sensitivity over the entire failure surface. This is graphically represented in Fig. 15. The symbols and solid line on the right figure represent the trajectory of the failure stress states produced by UD simple shear at different orientations according to the aforementioned analytical failure stress estimation method. The plot on the left-hand side highlights the available experimental stress states. Both results are overlaid on the local sensitivity distribution plot of the fitted Tsai-Wu model projected on the σ_{11}- σ_{22} plane. Since in the best scenario – at ca. 45-50° orientation – the failure stress state is situated on

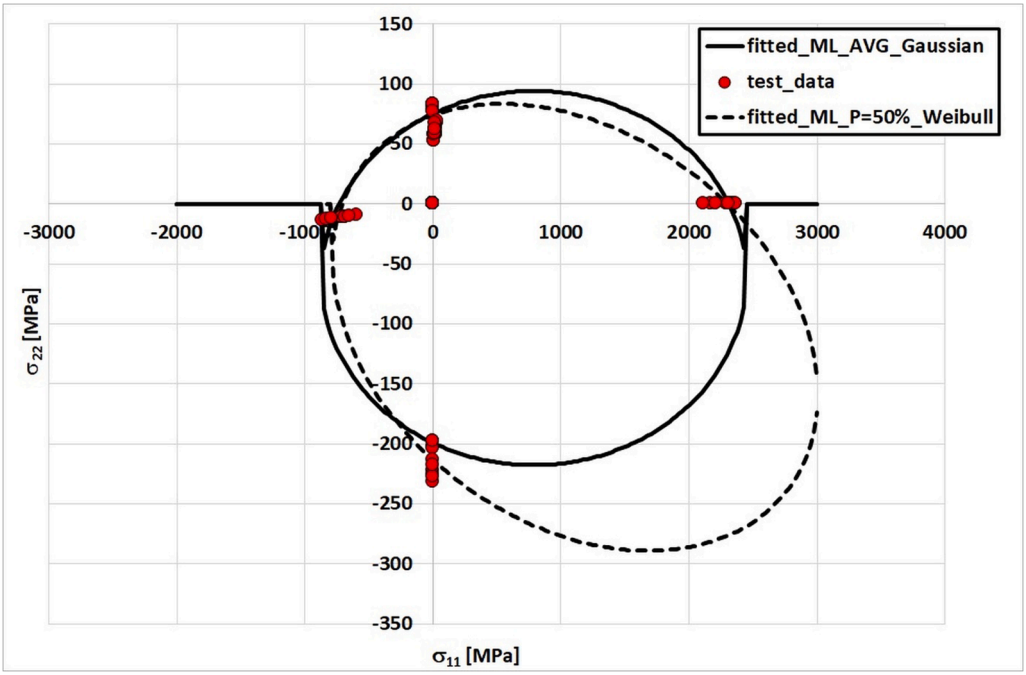

Fig. 10. Fitted Tsai-Wu failure envelope loci against real test data on σ_{11}- σ_{22} plane.

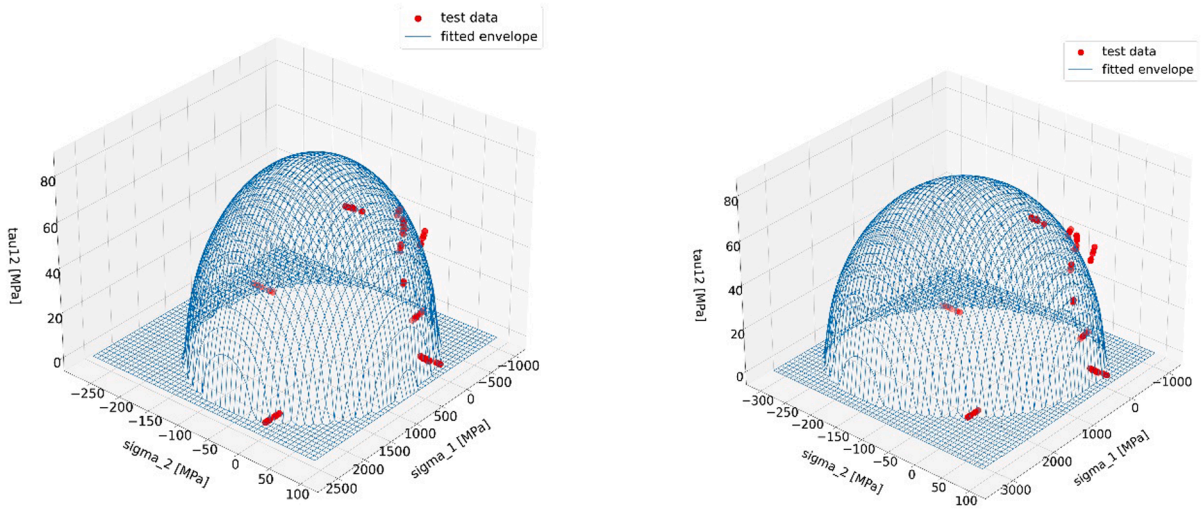

Fig. 11. Fitted Tsai-Wu failure envelopes against real test data in σ_{11}- σ_{22}- τ_{12} space assuming normal (left) and Weibull (right) strength CDF for MLE fit.

the border of the sensitive region in terms of the F_{12}* parameter, it is expected that a simple shear experiment with a 45-50° oriented plate would increase the robustness of the F_{12}* fit.

A possible simple shear test setup with inclined fiber directions is shown in Fig. 16. The specimen design and the entire setup are very similar to the V-notched specimen shear testing, however in this case there is a wider central section with a reduced width in order to generate a nearly homogeneous stress state in the weakest section which is also strongly influenced by the local fiber orientation. It must be emphasized, however, that the analytical DoE technique used here is only a tool for a crude conceptual predesign of the necessary mechanical experiment to provide more information about a failure model parameter to fit. In order to achieve a relatively homogeneous stress distribution in the measurement area, and also to understand the real failure stress state, detailed FEM assessment-based fixture design activity must be done.

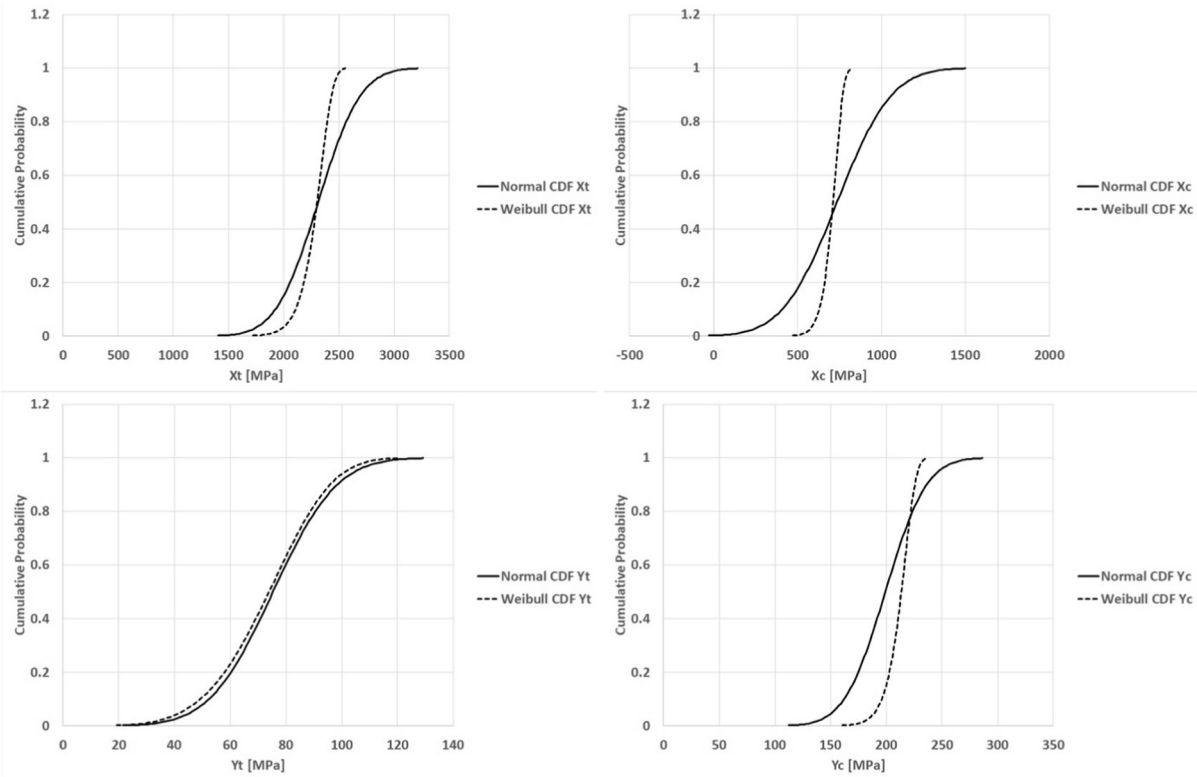

Fig. 12. Fitted strength CDFs assuming normal (solid) and Weibull (dashed) strength distributions.

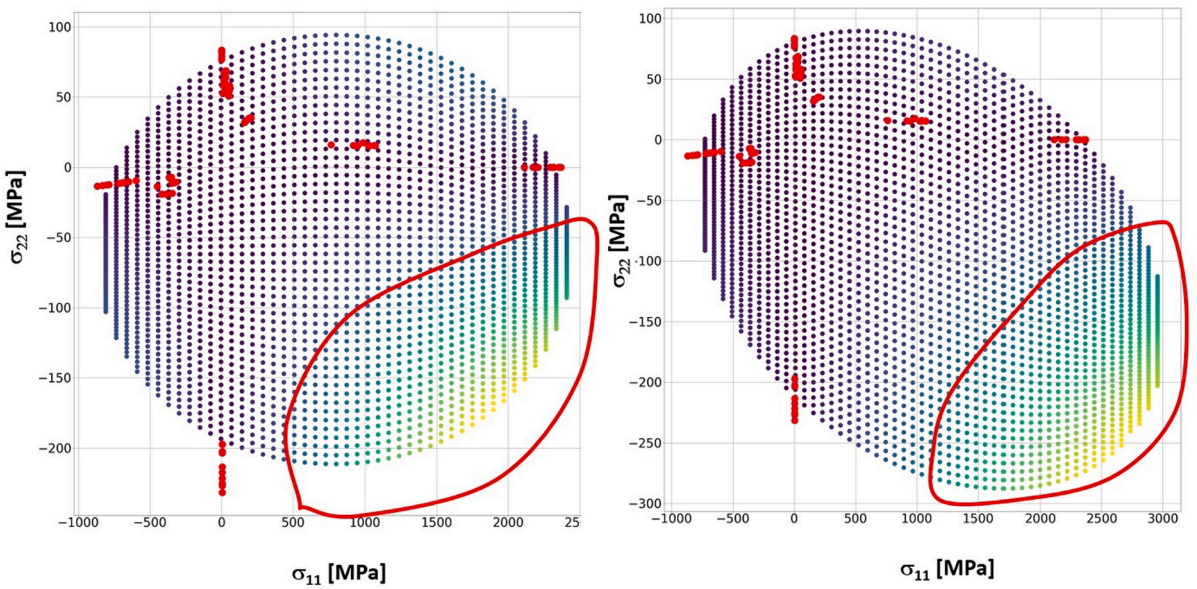

Fig. 13. Sensitivity distribution plots of F_{12}* parameter projected on σ_{11}- σ_{22} plane using normal (left) and Weibull (right) strength CDFs for model fit.

3.5. Evaluation of results based on existing literature

The methodology presented in this work attempts to assist engineers in making good decisions in two dilemmas: how to perform a robust first-ply failure model fit on available failure results as well as how to make sure that the available experimental data provides

enough information about all parameters of the targeted failure model. To demonstrate the added value of the presented methods, it was implemented on a set of experimental results via attempting to find the constants of the corresponding Tsai-Wu failure model. There is a rich literature available on the topic of finding F_{12}^*, thus, the outcome of the present experimental validation can be directly compared to the conclusions made in previous publications. The two types of results to compare are: 1) evaluated F_{12}^* against available suggested values and 2) recommended experiments and stress states for F_{12}^* evaluation against what is available in the literature.

In terms of both aspects [45] provides a good overview. In the work of Li [45] a deterministic formulation is provided for the Tsai-Wu constant as follows:

$$F_{12}^{*} = -0.5 \cdot \sqrt{\delta} \tag{25}$$

Where:

$$\delta = 4 - \frac{Y_t \cdot Y_c}{S_{23}^2} \tag{26}$$

Where S_{23} corresponds to the interlaminar shear strength in the 23 plane.

The deterministic calculation of F_{12}^* for the tested Toray CETEX TC1225 material was performed at different interlaminar shear strength levels which are shown in Fig. 17. However, the formula above can only be used for thermosetting matrix materials where $\delta < 0$. In that case, F_{12}^* can only take a negative value. Given that present fitted F_{12}^* values are close to zero or slightly positive it is expected that for this thermoplastic matrix FRPC the δ value is positive. According to [45] in that scenario clear suggestions or formulas for F_{12}^* cannot be given, as well as a fully open failure envelope is also possible. Thus, full deterministic proof for the fitted F_{12}^* for the tested FRPC with thermoplastic matrix could not be achieved.

In terms of identifiability of F_{12}^*, [45] provides an extensive review of the suggested stress states and potential mechanical experiments that may be used to estimate that. These stress states are graphically highlighted in the sensitivity plot generated for the tested Toray CETEX TC1225 material in Fig. 18. It follows clearly that none of the conventional off-axis or equibiaxial experiments on UD tapes produce a stress state situated in the vicinity of the highly sensitive zone.

According to the local sensitivity formula for the F_{12}^* parameter as per Equation (14), for maximizing it a stress state is desired where the product of σ_{11} and σ_{22} component magnitudes is the highest. Given that the analyzed UD tape is highly anisotropic, this stress state necessitates σ_{11} to be much higher than σ_{22}, and, since the compressive strength in the transverse direction is higher than in fiber direction, σ_{22} must be a large negative value. This is only possible in a tensile-compressive stress state dominated by a $\sigma_{11} > 0$ stress component. This fact precludes that equibiaxial states are suitable for highly anisotropic FRPC plies. Off-axis experiments of UD plates are also out of scope since in these scenarios the sign of σ_{11} and σ_{22} is identical. Thus, it can be concluded that none of the stress states connected with simple mechanical experiments suggested in the literature are suitable to robustly evaluate F_{12}^* based on the local sensitivity approach introduced in this work.

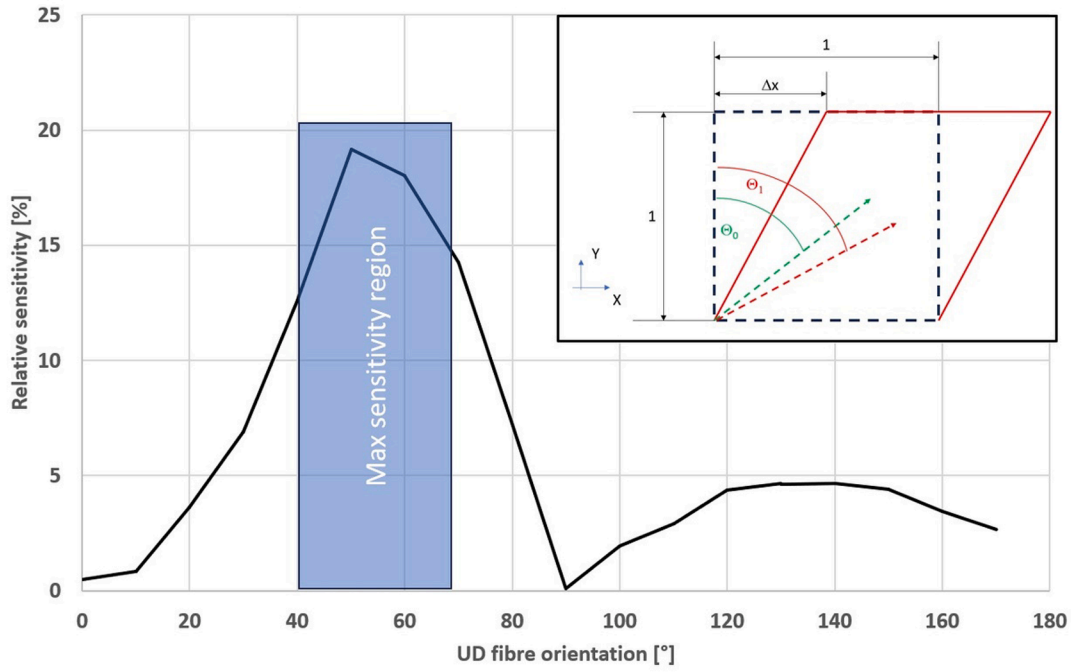

Fig. 14. Analytically estimated relative sensitivity to F_{12}^* parameter as a function of fiber orientation, simple shear experiment of UD sheet.

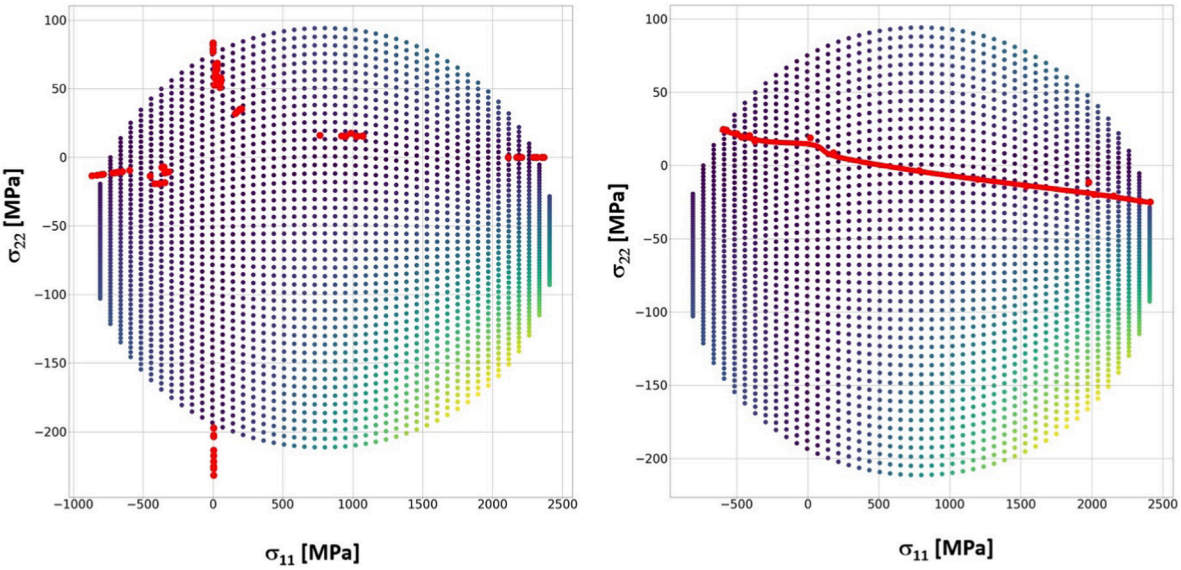

Fig. 15. Sensitivity distribution plots of F_{12}* parameter along with the available experimental failure stresses (left) and with the possible failure stress states from the simple shear experiment of UD sheet at different fiber orientations (right).

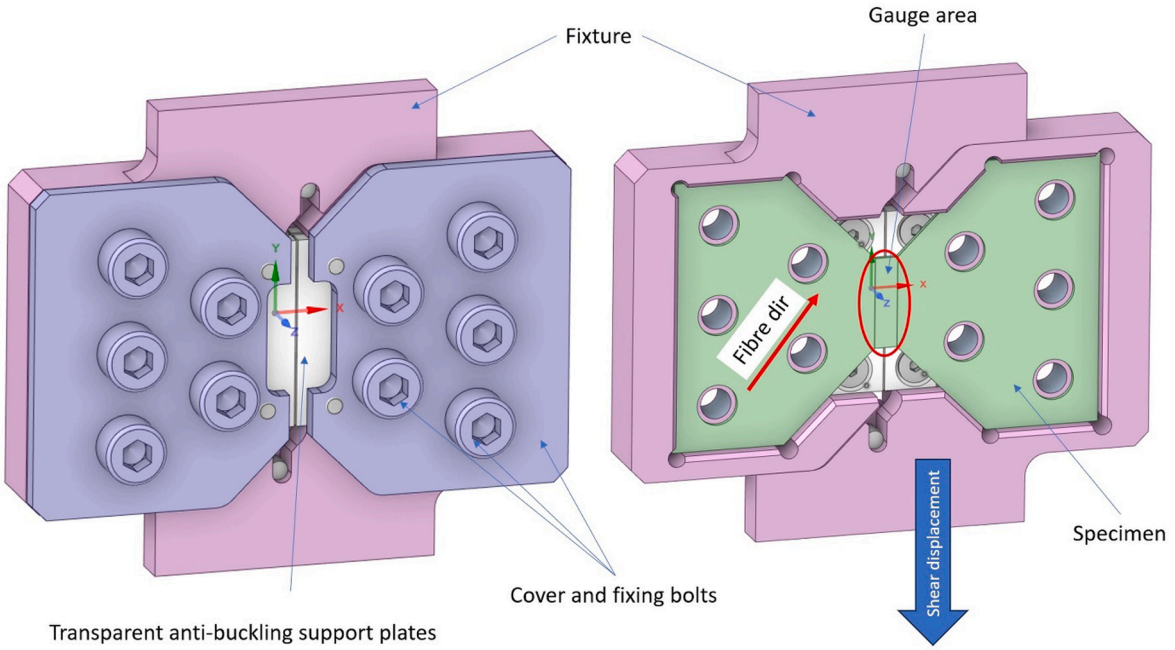

Fig. 16. Suggested simple shear test setup for V-notched composite UD plate with inclined fiber direction to deliver failure stress state for robust fit of F_{12}* constant.

Fig. 18 is clear evidence of the difficulty of experimental evaluation of F_{12}*. The simple shear experiment suggested in this work with 40-55° UD orientation generates the most information about F_{12}* amongst all relevant experiments, however, that is also relatively far from the potentially best σ_{11}- σ_{22} combination.

4. Conclusion

In this paper, a generic method was proposed for a holistic estimation of any preselected first-ply failure model parameters of a FRPC ply, combined with an analytical parameter identifiability study as well as further necessary mechanical experiment estimation.

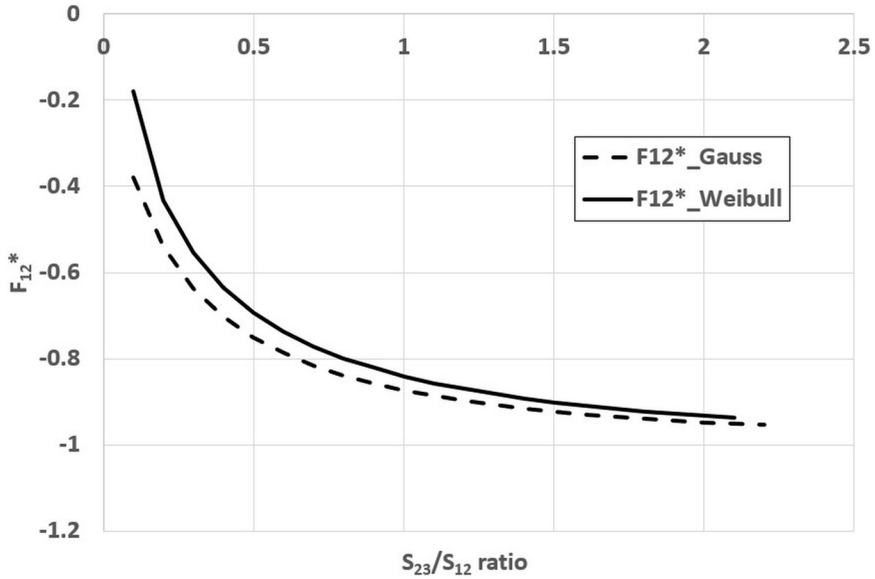

Fig. 17. F_{12}^* as a function of S_{23}/S_{12} ratio calculated with Equation (25) for $\delta < 0$ cases using fitted strength data from Section 3.2.

With the aid of this method, it becomes possible to perform a statistical fit on the strength data which significantly increases the applicability of experimentally deduced failure constants. This is because the Maximum Likelihood Estimation of the strength data returns Cumulative Distribution Functions.This allows quantifying the uncertainty about these parameters and also allows associating survival probability with the failure envelope parameters. This is a fundamental input into robustness analyses that pave the way for full virtualization of FRPC part design. The introduced methodology also provides means to figure out parameter identifiability from the available experiments. This is vital to avoid fake-fitted data due to lack of information. Information content of each experiment with regards to any failure model parameter is checked via local-sensitivity calculation. Finally, current work suggests a procedure to roughly estimate the most informative UD ply orientation for a preselected standard mechanical experiment setup.

The entire process was demonstrated and validated via processing numerous mechanical test results performed on Toray CETEX

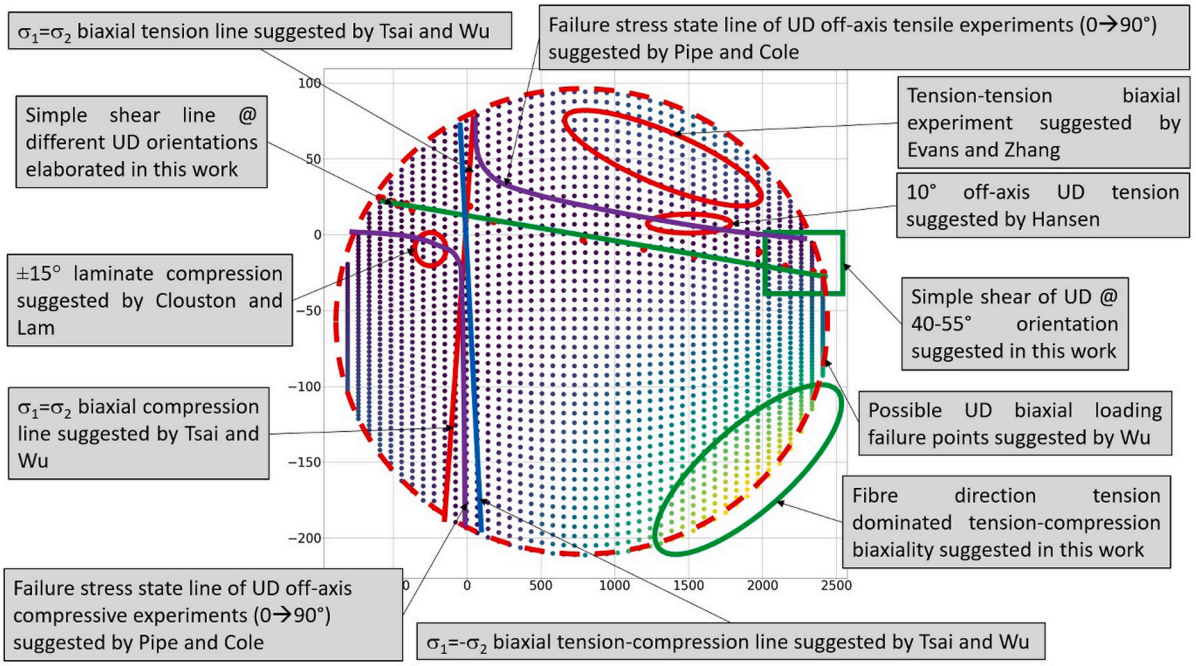

Fig. 18. Comparison of ideal σ_{11}- σ_{22} stress states for F_{12}^* evaluation overlaid on the sensitivity plot generated based on Toray CETEX TC1225 UD experiments.

TC1225 TP UD plies. The sensitivity analysis done on the stochastically fitted Tsai-Wu failure envelope parameters revealed that the F_{12}^* parameter was not identifiable with the available experimental data. To remedy this, the analytical DoE analysis was run for a simple shear experiment to find the most informative specimen fiber orientation that turned out to fall into the 40-60° domain. The outcome of this validation process was also compared against relevant literature results generated for typical thermosetting systems. The outcome is that the conventional parameters and experiments suggested for thermosetting systems are not guaranteed to be suitable for thermoplastic matrix FRPCs.

Prerequisites for the introduced methodology are the existence of a representative number of mechanical experiments as well as a suitable fitted material constitutive model for the plies. Lastly, FE analyses of each experiment need to be run and set up accordingly.

Declaration of competing interest

The authors declare that they have no known competing financial interests or personal relationships that could have appeared to influence the work reported in this paper.

Data availability

Data will be made available on request.

Acknowledgement

The project is funded by the National Research, Development and Innovation (NKFIH) Fund, Project title: Precision characterization of nonlinear mechanical behavior of reinforced and unreinforced polymeric materials for engineering simulations"; The application ID number: 2020-1.1.2-PIACI-KFI-2021-00314. The developers are grateful for the support.

References

[1] C.G. Soares, Reliability of components in composite materials, Reliab. Eng. Syst. Saf. 55 (2) (1997) 171–177, https://doi.org/10.1016/S0951-8320(96)00008-7.
[2] S. Sriramula, M.K. Chryssanthopoulos, Quantification of uncertainty modelling in stochastic analysis of FRP composites, Compos. Part A: Appl. Sci. Manuf. 40 (11) (2009) 1673–1684, https://doi.org/10.1016/j.compositesa.2009.08.020.
[3] M. Chiachio, J. Chiachio, G. Rus, Reliability in composites – A selective review and survey of current development, Compos. B Eng. 43 (3) (2012) 902–913, https://doi.org/10.1016/j.compositesb.2011.10.007.
[4] A.R. Melro, P.P. Camanho, S.T. Pinho, Generation of random distribution of fibres in long-fibre reinforced composites, Composites Science and Technology. 68 (9) (2008) 2092–2102, https://doi.org/10.1016/j.compscitech.2008.03.013.
[5] S. Behzadi, P. Curtis, F.R. Jones, Improving the prediction of tensile failure in unidirectional fibre composites by introducing matrix shear yielding, Compos. Sci. Technol. 69 (2009) 2421–2427, https://doi.org/10.1016/j.compscitech.2009.06.010.
[6] Y. Swolfs, L. Gorbatikh, V. Romanov, S. Orlova, S.V. Lomov, I. Verpoest, Stress concentrations in an impregnated fibre bundle with random fibre packing, Compos. Sci. Technol. 74 (2013) 113–120, https://doi.org/10.1016/j.compscitech.2012.10.013.
[7] Y. Swolfs, I. Verpoest, L. Gorbatikh, Issues in strength models for unidirectional fibre-reinforced composites related to Weibull distributions, fibre packings and boundary effects, Compos. Sci. Technol. 114 (2015) 42–49, https://doi.org/10.1016/j.compscitech.2015.04.002.
[8] S. Hussain, A. Dickson, Improving and predicting the mechanical properties of foamed and stretched composite poly(Lactic acid) films, Express Polym Lett 13 (2019) 18–26, https://doi.org/10.3144/expresspolymlett.2019.3.
[9] T.Y. Kam, E.S. Chang, Reliability formulation for composite laminates subjected to first-ply failure, Compos. Struct. 38 (1) (1997) 447–452, https://doi.org/10.1016/S0263-8223(97)00079-2.
[10] S.C. Lin, T.Y. Kam, K.H. Chu, Evaluation of buckling and first-ply failure probabilities of composite laminates, Int. J. Solids Struct. 35 (13) (1998) 1395–1410, https://doi.org/10.1016/S0020-7683(97)00113-3.
[11] S.C. Lin, T.Y. Kam, Probabilistic Failure Analysis of Transversely Loaded Laminated Composite Plates Using First-Order Second Moment Method, J. Eng. Mech. 126 (8) (2000) 812–820, https://doi.org/10.1061/(ASCE)0733-9399(2000)126:8(812).
[12] H.K. Jeong, R.A. Shenoi, Probabilistic strength analysis of rectangular FRP plates using Monte Carlo simulation, Comput. Struct. 76 (1) (2000) 219–235, https://doi.org/10.1016/S0045-7949(99)00171-6.
[13] A. Lal, B.N. Singh, D. Patel, Stochastic nonlinear failure analysis of laminated composite plates under compressive transverse loading, Compos. Struct. 94 (3) (2012) 1211–1223, https://doi.org/10.1016/j.compstruct.2011.11.018.
[14] A.M. Gadade, A. Lal, B.N. Singh, Accurate stochastic initial and final failure of laminated plates subjected to hygro-thermo-mechanical loadings using Puck's failure criteria, Int. J. Mech. Sci. 114 (2016) 177–206, https://doi.org/10.1016/j.ijmecsci.2016.05.015.
[15] S.P. Yushanov, A.E. Bogdanovich, Analytical probabilistic modeling of initial failure and reliability of laminated composite structures, Int. J. Solids Struct. 35 (7) (1998) 665–685, https://doi.org/10.1016/S0020-7683(97)00081-4.
[16] A. Shaw, S. Sriramula, P.D. Gosling, M.K. Chryssanthopoulos, A critical reliability evaluation of fibre reinforced composite materials based on probabilistic micro and macro-mechanical analysis, Compos. B Eng. 41 (6) (2010) 446–453, https://doi.org/10.1016/j.compositesb.2010.05.005.
[17] X.Y. Zhou, P.D. Gosling, Z. Ullah, L. Kaczmarczyk, C.J. Pearce, Stochastic multi-scale finite element based reliability analysis for laminated composite structures, App. Math. Model. 45 (2017) 457–473, https://doi.org/10.1016/j.apm.2016.12.005.
[18] S.C. Lin, Reliability predictions of laminated composite plates with random system parameters, Probab. Eng. Mech. 15 (4) (2000) 327–338, https://doi.org/10.1016/S0266-8920(99)00034-X.
[19] S.C. Lin, Buckling failure analysis of random composite laminates subjected to random loads, Int. J. Solids Struct. 37 (51) (2000) 7563–7576, https://doi.org/10.1016/S0020-7683(99)00305-4.
[20] M.B. Whiteside, S.T. Pinho, P. Robinson, Stochastic failure modelling of unidirectional composite ply failure, Reliab. Eng. Syst. Saf. 108 (2012) 1–9, https://doi.org/10.1016/j.ress.2012.05.006.
[21] L. Zhao, M. Shan, F. Liu, J. Zhang, A probabilistic model for strength analysis of composite double-lap single-bolt joints, Compos. Struct. 161 (2017) 419–427, https://doi.org/10.1016/j.compstruct.2016.11.074.
[22] J.C. Helton, F.J. Davis, Latin hypercube sampling and the propagation of uncertainty in analyses of complex systems, Reliab. Eng. Syst. Saf. 81 (1) (2003) 23–69, https://doi.org/10.1016/S0951-8320(03)00058-9.
[23] M.J. Bogdanor, C. Oskay, S.B. Clay, Multiscale modeling of failure in composites under model parameter uncertainty, Comput. Mech. 56 (3) (2015) 389–404, https://doi.org/10.1007/s00466-015-1177-7.

[24] C.A. Conceição António, A hierarchical genetic algorithm for reliability based design of geometrically non-linear composite structures, Compos. Struct. 54 (1) (2001) 37–47, https://doi.org/10.1016/S0263-8223(01)00068-X.
[25] G. Soremekun, Z. Gürdal, R.T. Haftka, L.T. Watson, Composite laminate design optimization by genetic algorithm with generalized elitist selection, Comput. Struct. 79 (2) (2001) 131–143, https://doi.org/10.1016/S0045-7949(00)00125-5.
[26] M. Walker, R.E. Smith, A technique for the multiobjective optimisation of laminated composite structures using genetic algorithms and finite element analysis, Compos. Struct. 62 (1) (2003) 123–128, https://doi.org/10.1016/S0263-8223(03)00098-9.
[27] C.H. Park, W.I. Lee, W.S. Han, A. Vautrin, Improved genetic algorithm for multidisciplinary optimization of composite laminates, Comput. Struct. 86 (19) (2008) 1894–1903, https://doi.org/10.1016/j.compstruc.2008.03.001.
[28] F.S. Almeida, A.M. Awruch, Design optimization of composite laminated structures using genetic algorithms and finite element analysis, Compos. Struct. 88 (3) (2009) 443–454, https://doi.org/10.1016/j.compstruct.2008.05.004.
[29] P.A.M. Lopes, H.M. Gomes, A.M. Awruch, Reliability analysis of laminated composite structures using finite elements and neural networks, Compos. Struct. 92 (7) (2010) 1603–1613, https://doi.org/10.1016/j.compstruct.2009.11.023.
[30] H.M. Gomes, A.M. Awruch, P.A.M. Lopes, Reliability based optimization of laminated composite structures using genetic algorithms and Artificial Neural Networks, Struct. Saf. 33 (3) (2011) 186–195, https://doi.org/10.1016/j.strusafe.2011.03.001.
[31] R. Ge, J. Chen, J. Wei, Reliability-based design of composites under the mixed uncertainties and the optimization algorithm, Acta Mechanica Solida Sinica. 21 (1) (2008) 19–27, https://doi.org/10.1007/s10338-008-0804-7.
[32] J. Chen, Y. Tang, R. Ge, Q. An, X. Guo, Reliability design optimization of composite structures based on PSO together with FEA, Chin. J. Aeronaut. 26 (2) (2013) 343–349, https://doi.org/10.1016/j.cja.2013.02.011.
[33] S.W. Tsai, E.M. Wu, A General Theory of Strength for Anisotropic Materials, J. Compos. Mater. 5 (1) (1971) 58–80, https://doi.org/10.1177/002199837100500106.
[34] O. Hoffman, The Brittle Strength of Orthotropic Materials, J. Compos. Mater. 1 (2) (1967) 200–206, https://doi.org/10.1177/002199836700100210.
[35] Z. Hashin, Failure Criteria for Unidirectional Fiber Composites, J. Appl. Mech. 47 (2) (1980) 329–334, https://doi.org/10.1115/1.3157744.
[36] A. Puck, H. Schürmann, Failure analysis of FRP laminates by means of physically based phenomenological models, Compos. Sci. Technol. 62 (12) (2002) 1633–1662, https://doi.org/10.1016/S0266-3538(01)00208-1.
[37] R.G. Cuntze, A. Freund, Chapter 3.14 - The predictive capability of failure mode concept-based strength criteria for multidirectional laminates, in: M.J. Hinton, A.S. Kaddour, P.D. Soden (Eds.), Failure Criteria in Fibre-Reinforced-Polymer Composites, Elsevier, Oxford, 2004, pp. 429–489, https://doi.org/10.1016/S0266-3538(03)00225-2.
[38] C. Dávila, P. Camanho, C. Rose, Failure Criteria for FRP Laminates, J. Compos. Mater. (2005) 39, https://doi.org/10.1177/0021998305046452.
[39] Pinho S, Dávila C, Camanho P, Iannucci L, Robinson P. Failure Models and Criteria for FRP Under In-Plane or Three-Dimensional Stress States Including Shear Non-Linearity. 2005.
[40] M.J. Hinton, P.D. Soden, Predicting failure in composite laminates: the background to the exercise, Compos. Sci. Technol. 58 (7) (1998) 1001–1010, https://doi.org/10.1016/S0266-3538(98)00074-8.
[41] Hinton M, Kaddour AS, Soden P. Failure Criteria in Fibre-Reinforced-Polymer Composites: The World-Wide Failure Exercise2004.
[42] M. Hinton, A. Kaddour, The background to the Second World-Wide Failure Exercise, J. Compos. Mater. 46 (19–20) (2012) 2283–2294, https://doi.org/10.1177/0021998312449885.
[43] A. Kaddour, M. Hinton, P. Smith, S. Li, The background to the third world-wide failure exercise, J. Compos. Mater. 47 (20–21) (2013) 2417–2426, https://doi.org/10.1177/0021998313499475.
[44] S.R. Soni, A Comparative Study of Failure Envelopes in Composite Laminates, J. Reinf. Plast. Compos. 2 (1) (1983) 34–42, https://doi.org/10.1177/073168448300200104.
[45] S. Li, E. Sitnikova, Y. Liang, A.-S. Kaddour, The Tsai-Wu Failure Criterion Rationalised in the Context of UD Composites 102: (2017) 207–217.
[46] S.J. Deteresa, G.J. Larsen, Derived Interaction Parameters for the Tsai-Wu Tensor Polynomial Theory of Strength for Composite Materials, American Society of Mechanical Engineers, Applied Mechanics Division, AMD. 248 (2001), https://doi.org/10.1115/IMECE2001/AMD-25417.
[47] S. Li, M. Xu, E. Sitnikova, The Formulation of the Quadratic Failure Criterion for Transversely Isotropic Materials: Mathematical and Logical Considerations, Journal of Composites Science. 6 (3) (2022) 82, https://doi.org/10.3390/jcs6030082.
[48] P. Clouston, F. Lam, J.D. Barrett, Interaction Term of Tsai-Wu Theory for Laminated Veneer, J. Mater. Civ. Eng. 10 (2) (1998) 112–116, https://doi.org/10.1061/(ASCE)0899-1561(1998)10:2(112).
[49] A. F. Bower. Applied Mechanics of Solids. Taylor & Francis Inc, 2009.
[50] R. D. Cook, D. S. Malkus, M. E. Plesha, R. J. Witt. Concepts and Applications of Finite Element Analysis, 4th Edition, 2001.
[51] L P Kollár, G S Springer: Mechanics of Composite Structures. Cambridge University Press, 2009.
[52] W. Mascarenhas, C. Ahrens, A. Ogliari, Design criteria and safety factors for plastic components design, Mater. Des. 25 (2004) 257–261, https://doi.org/10.1016/j.matdes.2003.10.003.
[53] A.T. Echtermeyer, K. Lasn, Safety approach for composite pressure vessels for road transport of hydrogen. Part 2: Safety factors and test requirements, Int. J. Hydrogen Energy 39 (26) (2014) 14142–14152, https://doi.org/10.1016/j.ijhydene.2014.06.016.
[54] L.-S. Wang, Z.-M. Huang, On strength prediction of laminated composites. Composite, Sci. Technol. (2022) 219, https://doi.org/10.1016/j.compscitech.2021.109206.
[55] T.S. Mesogitis, A.A. Skordos, A.C. Long, Uncertainty in the manufacturing of fibrous thermosetting composites: A review, Compos. A Appl. Sci. Manuf. 57 (2014) 67–75, https://doi.org/10.1016/j.compositesa.2013.11.004.
[56] MIL-HDBK-17-1F (2002). Composite Materials Handbook: Volume 1. Polymer Matrix Composites Guidelines for Characterization of Structural Materials, Department of Defense Handbook., 1: Chapter 7.
[57] S. Li, Z.Y. Ma, Strength Analysis of Multidirectional Fiber-Reinforced Composite Laminates with Uncertainty in Macromechanical Properties, Physical Mesomechanics 24 (2021) 311–318, https://doi.org/10.1134/S1029959921030097.
[58] D.M. Takács, Sz. Berezvai, L. Kovács, A general method for numerical identifiability and sensitivity analysis of failure criteria for continuous fibre-reinforced plastics, European Journal of Mechanics / A Solids (2023) 100, https://doi.org/10.1016/j.euromechsol.2023.104976.
[59] A.C. Orifici, I. Herszberg, R.S. Thomson, Review of methodologies for composite material modelling incorporating failure, Compos. Struct. 86 (1–3) (2008) 194–210, https://doi.org/10.1016/j.compstruct.2008.03.007.
[60] Wan, L., Ullah, Z., & Falzon, B. G. (2022). Failure criteria assessment of composite materials via micromechanics modelling under multiaxial loading conditions. In A. P. Vassilopoulos, & V. Michaud (Eds.), Proceedings of the 20th European Conference on Composite Materials (ECCM20): Composites meet sustainability (Vol. 4 (D), pp. 26-33). (European Conference on Composite Materials: Proceedings). MDPI AG.
[61] E. Totry, C. González, J. Llorca, Prediction of the failure locus of C/PEEK composites under transverse compression and longitudinal shear through computational micromechanics, Composite Science and Technology 68 (2008) 3128–3136, https://doi.org/10.1016/j.compscitech.2008.07.011.
[62] M. V. Donadon, S. F. M. de Almeida, M. A. Arbelo, A. R. de Faria. A Three-Dimensional Ply Failure Model for Composite Structures. International Journal of Aerospace Engineering. 2009; Article ID 486063, 22 pages. 10.1155/2009/486063.
[63] I.J. Myung, Tutorial on maximum likelihood estimation, J. Math. Psychol. 47 (1) (2003) 90–100, https://doi.org/10.1016/S0022-2496(02)00028-7.
[64] W. Navidi, Statistics for Engineers and Scientists, 5th Edition,, McGraw Hill Higher Education, 2020.
[65] Q.S. Zheng, Q.C. He, A. Curnier, Simple shear decomposition of the deformation gradient, Acta Mechanica. 140 (2000) 131–147, https://doi.org/10.1007/BF01182506.